A EUROPEAN JOURNAL OF CHEMICAL BIOLOGY

CHEMBIOCHEM

SYNTHETIC BIOLOGY & BIO-NANOTECHNOLOGY

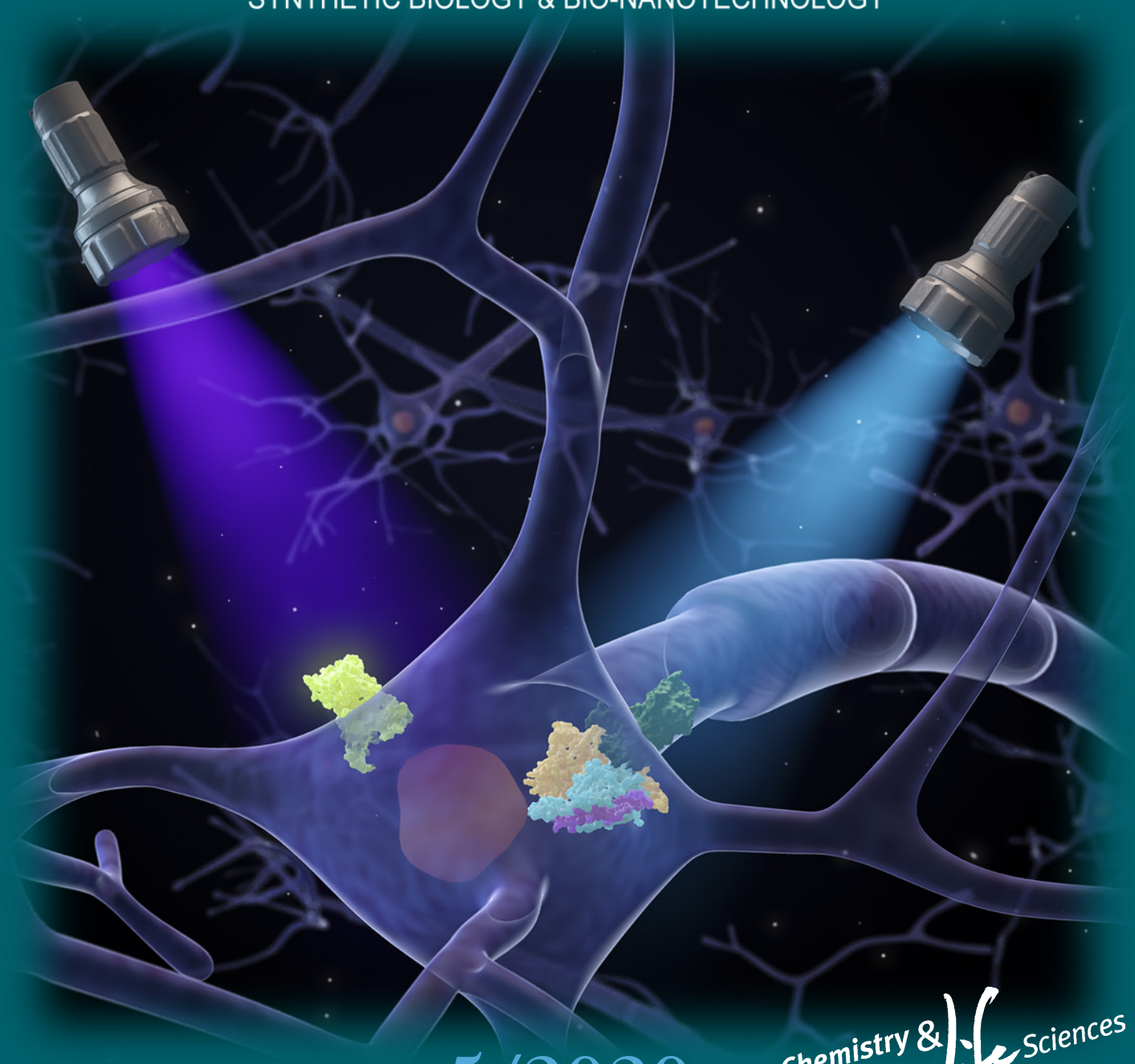

5/2020

Chemistry & Life Sciences

Front Cover:
D. Eickelbeck, K. Gerwert, S. Herlitze et al.
Lamprey Parapinopsin ("UVLamP"): A Bistable UV-Sensitive Optogenetic Switch for Ultrafast Control of GPCR Pathways

A Journal of
ChemPubSoc Europe

WILEY-VCH

www.chembiochem.org

ChemPubSoc Europe

DOI: 10.1002/cbic.201900485

CHEMBIOCHEM Communications

VIP *Very Important Paper*

Lamprey Parapinopsin ("UVLamP"): a Bistable UV-Sensitive Optogenetic Switch for Ultrafast Control of GPCR Pathways

Dennis Eickelbeck,*[a] Till Rudack,[b, c] Stefan Alexander Tennigkeit,[b, c] Tatjana Surdin,[a] Raziye Karapinar,[a] Jan-Claudius Schwitalla,[a] Brix Mücher,[a] Maiia Shulman,[b, c] Marvin Scherlo,[b, c] Philipp Althoff,[b, c] Melanie D. Mark,[a] Klaus Gerwert,*[b, c] and Stefan Herlitze[a]

Optogenetics uses light-sensitive proteins, so-called optogenetic tools, for highly precise spatiotemporal control of cellular states and signals. The major limitations of such tools include the overlap of excitation spectra, phototoxicity, and lack of sensitivity. The protein characterized in this study, the Japanese lamprey parapinopsin, which we named UVLamP, is a promising optogenetic tool to overcome these limitations. Using a hybrid strategy combining molecular, cellular, electrophysiological, and computational methods we elucidated a structural model of the dark state and probed the optogenetic potential of UVLamP. Interestingly, it is the first described bistable vertebrate opsin that has a charged amino acid interacting with the Schiff base in the dark state, that has no relevance for its photoreaction. UVLamP is a bistable UV-sensitive opsin that allows for precise and sustained optogenetic control of G protein-coupled receptor (GPCR) pathways and can be switched on, but more importantly also off within milliseconds via low-intensity short light pulses. UVLamP exhibits an extremely narrow excitation spectrum in the UV range allowing for sustained activation of the $G_{i/o}$ pathway with a millisecond UV light pulse. Its sustained pathway activation can be switched off, surprisingly also with a millisecond blue light pulse, minimizing phototoxicity. Thus, UVLamP serves as a minimally invasive, narrow-bandwidth probe for controlling the $G_{i/o}$ pathway, allowing for combinatorial use with multiple optogenetic tools or sensors. Because UVLamP activated $G_{i/o}$ signals are generally inhibitory and decrease cellular activity, it has tremendous potential for health-related applications such as relieving pain, blocking seizures, and delaying neurodegeneration.

Using light to control cellular signals has already been suggested 40 years ago in 1979 by Crick, who imagined that neuronal excitability could be controlled via light with much more spatiotemporal precision than with pharmacological or electrical approaches. Starting with the expression of microbial and animal opsins in neurons, the field of optogenetics has been developed in the last two decades.[1] Optogenetics uses the combination of optical, genetic and viral methods to achieve control of cellular states, function and signaling with unmatched spatial and temporal precision.[2] Often so-called opsins, a class of light-sensitive proteins, are used to optogenetically control cellular functions ranging from in vitro assays to control of complex behavioral tasks in freely moving animals. Typically, these opsins are expressed in genetically precisely targeted cell populations, for example, by viral transduction and can then be used to exclusively modulate the desired cell population in multiple ways via application of light pulses. Opsins can be classified into type I (microbial) and type II (animal) opsins with type I opsins being employed by prokaryotes, fungi and algae and type II opsins being found in animals.[3] Type II opsins belong to the seven-transmembrane-domain (7TM) GPCR superfamily, with most being typical light-sensitive GPCRs, consisting of a 7TM protein moiety (opsin) and a light-sensing non-protein moiety (the chromophore retinal).[4] The retinal itself is bound to the protein moiety through a protonated Schiff base (SB) linkage. This binding site is energetically unstable and has to be stabilized by a counterion in the protein interior. There are two tentative sites that can serve as a counterion: E113 in transmembrane helix 3 and E181 in extracellular loop 2 (positions for bovine rhodopsin). For monostable (commonly vertebrate) opsins this counterion

[a] *D. Eickelbeck, T. Surdin, R. Karapinar, Dr. J.-C. Schwitalla, B. Mücher, Dr. M. D. Mark, Prof. Dr. S. Herlitze*
Department of General Zoology and Neurobiology, Ruhr University Bochum
ND7/31, Universitätsstasse 150, 44780 Bochum (Germany)
E-mail: dennis.eickelbeck@rub.de

[b] *Dr. T. Rudack, Dr. S. A. Tennigkeit, M. Shulman, M. Scherlo, P. Althoff, Prof. Dr. K. Gerwert*
Biospectroscopy, Center for Protein Diagnostics (ProDi)
Ruhr University Bochum
Gesundheitscampus 4, 44801 Bochum (Germany)
E-mail: gerwert@bph.rub.de

[c] *Dr. T. Rudack, Dr. S. A. Tennigkeit, M. Shulman, M. Scherlo, P. Althoff, Prof. Dr. K. Gerwert*
Department of Biophysics, Ruhr University Bochum
ND04/596, Universitätsstrasse 150, 44780 Bochum (Germany)

Supporting information and the ORCID identification numbers for the authors of this article can be found under https://doi.org/10.1002/cbic.201900485.

is typically E113, whereas bistable (commonly invertebrate) opsins usually employ the more ancestral E181 as their counterion.[3,5] Interestingly, in the dark state structure of both vertebrates[6] and invertebrates[6] the analogues to positions 113 interact with the SB. It is assumed that within the photo cycle rearrangements in extracellular loop 2 lead to a change in the interaction network of the SB.[7]

Here we biophysically characterized the Japanese lamprey (*Lethenteron camtschaticum*) parapinopsin, a natively G_t-coupled, UV-sensitive, vertebrate nonvisual type II opsin. We reveal its capability to control the $G_{i/o}$ signaling pathway with unseen unique features making it an ideal optogenetic tool for multiple applications in particular in the brain.

GPCRs coupling to the $G_{i/o}$ signaling pathways in the brain are inhibitory. They are therefore gatekeepers of brain function by reducing neuronal excitability and keeping the brain in balance during emotion and arousal, contributing to neuronal plasticity during development, learning and memory formation. The main and modulatory transmitter systems such as glutamate, GABA, serotonin, dopamine, Ach, adrenaline and noradrenaline rely on negative feedback mechanisms using GPCRs coupling to the $G_{i/o}$ pathway and therefore represent major drug targets of the pharmaceutical industry.[8] These pathways can now be controlled in a highly precise manner using parapinopsin.

Japanese lamprey parapinopsin (hereafter: UVLamP or parapinopsin) is a homologue of the first identified catfish parapinopsin, which was detected in the catfish pineal complex.[9] Parapinopsin homologues have been found in the pineal organ and its related organs of lower vertebrates.[10] They have been found to couple to the G_t pathway and to be involved in extraretinal photoreception, especially in color discrimination between UV and visible light due to their bistable nature, with the optogenetic potential of parapinopsin being first proposed in 2015.[11,12]

Recently, we characterized mouse and human homologues of melanopsin, another non-visual opsin that can be found in intrinsically photosensitive retinal ganglion cells (ipRGCs) of the vertebrate retina and is involved in multiple physiological processes, for example, the circadian rhythm. We could show that melanopsin is a bistable/tristable opsin and a unique optogenetic tool that can be switched on/off with blue/green light pulses and can precisely control the $G_{i/o}$ and G_q pathway in different expression systems like the mouse brain.[13,14] Despite its advantageous characteristics, like high light sensitivity, bistable switching between sustained active and inactive states with short light pulses and strong expression in different systems, two drawbacks remained: First, melanopsin is activated/deactivated in the visible spectrum ranging from blue for activation to green/yellow for deactivation, therefore overlapping with most other optogenetic tools. Second, depending on the expression system, melanopsin is capable of activating two different G protein pathways, namely the $G_{i/o}$ and the G_q pathway, making it potentially imprecise for specific pathway control experiments. Herein, we show that UVLamP overcomes these drawbacks making it an ideal next generation optogenetic tool, especially for applications involving multi tool expression and highly precise control of distinct G protein pathways.

Lamprey parapinopsin induces a light-dependent hyperpolarization response in photoreceptor cells of the pineal organ and inhibits adenylyl cyclase-dependent cAMP responses in HEK 293S cells,[11,12] thus suggesting the activation of the $G_{i/o}$ pathway. Therefore, we characterized the light-dependent responses on $G_{i/o}$-mediated activation and deactivation of GIRK currents, using HEK 293 cells that stably express G protein-coupled inwardly rectifying K^+ (GIRK) channels,[15] which has been shown to be an ideal system for precise characterization of light-induced $G_{i/o}$ pathway activation and deactivation[13,15–17] GIRK channels are modulated through the $G_{i/o}$ pathway via fast direct interaction with G protein $\beta\gamma$-subunits leading to the hyperpolarization of the cell membrane in brain and heart.[16] We found that, like other G_t coupled photoreceptors derived from rods and cones, UVLamP effectively activates $G_{i/o}$-mediated GIRK channels. UVLamP induces sustained $G_{i/o}$-dependent GIRK currents (Figures 1 and 3 A) through a 100 ms UV light pulse (360 nm, 0.5 mW m^{-2}) that can be completely deactivated with another 100 ms blue light pulse (470 nm, 0.5 mW m^{-2}; Figure 1 A). Thus, UVLamP demands much shorter light pulses for switching between active and inactive states in comparison for example to bistable mouse melanopsin that needs several seconds of constant light stimulation for a full deactivation.[13] We used this direct GIRK channel modulation to electrophysiologically characterize the action spectrum of UVLamP rather than biochemically measuring the absorption spectrum. Characterizing the action spectrum is much more sensitive and involves functional GPCR pathway activation as a readout.[18] We found that UVLamP displays a strongly UV-shifted and narrow excitation (action) spectrum as it is exclusively activated by UV light below 410 nm with a maximum activation efficiency between 360–370 nm and can be deactivated with blue/green light between 440–570 nm with a maximum deactivation efficiency in the blue range between 470–510 nm (Figure 1 B). Additionally, UVLamP can be repetitively activated with minimal decline in response amplitude (Figure 1 D).

So far, the 3D structure of the Japanese lamprey parapinopsin (UVLamP) has not been determined. Here, we constructed in silico an atomistic model of membrane inserted solvated parapinopsin in complex with GDP bound $G_{i/o}$ protein, reflecting the dark state structure. To this end, we employed the modeling concept we recently developed to build and validate an atomic model of melanopsin[14] as outlined under Model construction and Model validation in the Supporting Information. The X-ray structure of bovine rhodopsin (PDB ID: 1U19)[19] served as a basis to build parapinopsin. The X-ray structures of the heterotrimeric $G_{i/o}$ protein with PDB IDs 1GP2[20] and 1BOF[21] were used to complete the binary complex. The sequence alignment shown in Figure S2 in the Supporting Information reveals that the similarity between parapinopsin and bovine rhodopsin is sufficient to build a reliable model exhibiting a similarity of 66% within the modeled sequence region (Table S1).

The resulting structural model shown in Figure 2 A was then used to initiate a 475 ns molecular mechanics (MM) simulation.

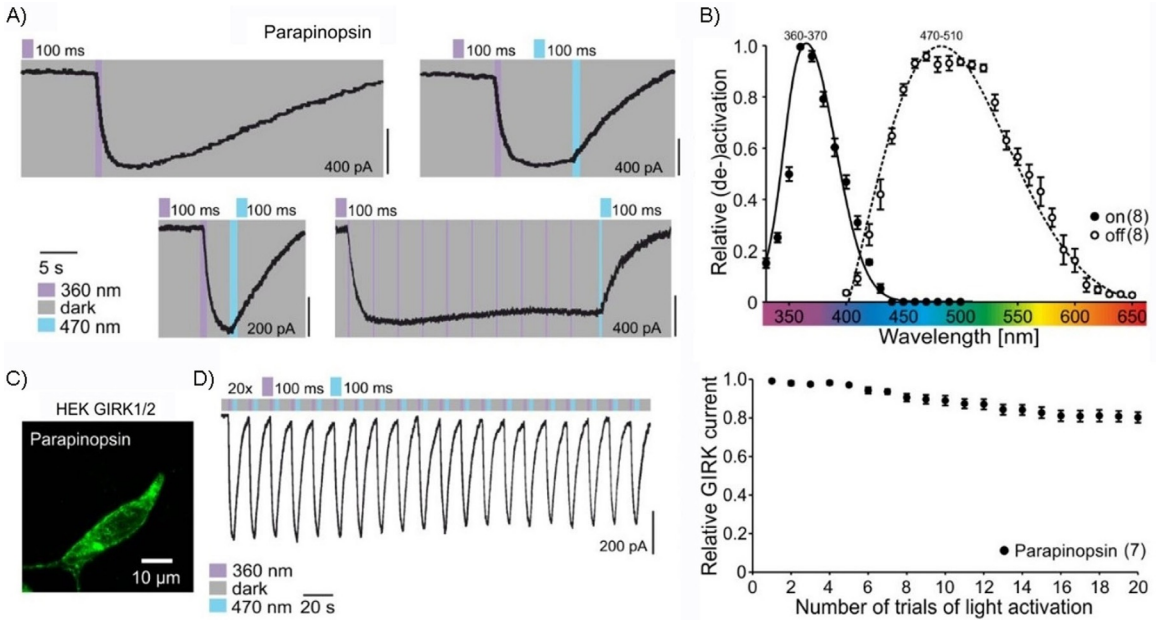

Figure 1. In vitro characterization of Japanese lamprey parapinopsin ("UVLamP") via whole-cell patch-clamp recordings of GIRK currents in HEK GIRK 1/2 cells. a) UVLamP induces sustained $G_{i/o}$-mediated GIRK currents via millisecond UV light stimulation that can be deactivated via millisecond blue light stimulation. b) Action spectra depicting the wavelength dependence of UVLamP activation and deactivation. c) Expression of UVLamP (*L. camtschaticum* parapinopsin-eGFP) in HEK cells. d) Repetitive (de-)activation of UVLamP.

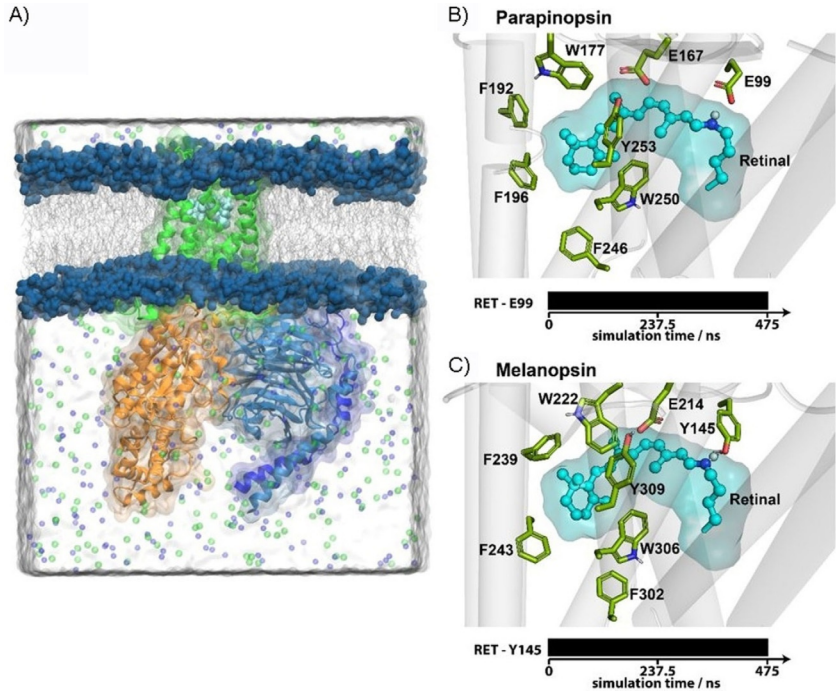

Figure 2. In silico characterization of parapinopsin in comparison with melanopsin. a) Simulation system of a membrane inserted solvated parapinopsin (green) $G_{i/o}$ protein complex. Illustrated at right are the representative structures of the retinal (cyan) binding pocket of b) parapinopsin and c) melanopsin of the converged MD simulation. Amino acids interacting with the retinal are highlighted as sticks. The contact pattern over the simulation time of the interaction partners of the SB is shown below as bar.

The protein backbone forming Cα atom positions converged after 350 ns as reflected by their root-mean-square deviation (RMSD) shown in Figure S7. Thus, we consider the obtained equilibrated trajectory as stable and reliable conformation, reflecting the dynamic interaction network of dark state parapinopsin. Next, we compared the dynamics of the interaction network of parapinopsin in detail with those derived from melanopsin MD simulations. The comparison of a representative dark state structure of the converged retinal binding pockets of parapinopsin and melanopsin is shown in Figure 2B,C. Inter-

estingly, the models show that despite their high identity within the retinal binding pocket the key binding partner of the retinal SB is different. In parapinopsin a glutamate (E99 (E113 for bovine rhodopsin)) interacts with the SB in the dark state, in contrast to melanopsin where it is a tyrosine (Y145 (E113 for bovine rhodopsin)). Within both proteins the E99 or Y145 interact with the SB over the whole simulation trajectory which indicates very strong binding. This is of particular interest because for other bistable vertebrate opsins except for encephalopsin,[22] position 99 (113 for bovine rhodopsin) is typically occupied by neutral amino acid residues such as Y, F, M. Yet, parapinopsin employs glutamate at both positions 99 (113 for bovine rhodopsin) and 167 (181 for bovine rhodopsin) similar to monostable pigments like bovine rhodopsin.[3, 10, 23]

To identify the counterion, we created and electrophysiologically characterized mutations of the potential counterion sites at position E99 (E113 for bovine rhodopsin) and position E167 (E181 for bovine rhodopsin; Figure S1). Point mutations at both positions (E99A/H/Y, E167A/H/Y) showed that altering/removing the potential counterion at position E99 does not interfere with UVLamP functionality, whereas alterations at position E167 completely abolished its functionality (Figure S1). That E99 does not impact parapinopsin function is in contrast to melanopsin, where the mutation of the E99 analogue Y145 is functionally important. Mutation of Y145, despite not being a potential counterion, led to a total loss of melanopsin function,[24] while for encephalopsin the functional relevance of its analogous aspartate is still unknown.[12] The parapinopsin results show that E167 is the sole counterion for the photoproduct of UVLamP.[10] Thus, comparable with mouse melanopsin, the Japanese lamprey parapinopsin (UVLamP), despite belonging to the group of vertebrate opsins, still uses the ancestral invertebrate opsin counterion.

In conclusion, our electrophysiological data show that parapinopsin is bistable. Parapinopsin uses E167 (E181 for bovine rhodopsin) as a sole counterion, at least for the photoproduct, with mutations at position E99 having no impact on parapinopsin functionality. Complementary analysis of the contact network (Figure 2) within biomolecular simulations shows that E99 is strongly bound to the SB in the dark state. Therefore, our data imply that critical interaction of the amino acid residue at this position, in contrast to melanopsin, cannot be of relevance for parapinopsin bistability or functionality.

We further characterized the properties of light-induced $G_{i/o}$ signaling via UVLamP in detail in vitro and found that its light-induced activation and deactivation time constants with 1.15 s for activation and 4.95 s for deactivation (Figure 3A). These time constants are even faster than those of wild-type mouse melanopsin ($\approx$1.4 and $\approx$8.5 s, respectively[13]) and comparable with the recently engineered Y211F mutant.[14] We next investigated the minimal light pulse duration for activation and deactivation of GIRK channels using UVLamP. We found that 100 ms light pulses (360/470 nm) are sufficient for full activation and deactivation efficiency with half-maximal (de-)activation already occurring at 30 ms (Figure 3B), outperforming other GPCR-based optogenetic tools. Also optogenetically beneficial is the very high light sensitivity of UVLamP (Figure 3C), which reaches maximal activation and deactivation by 100 ms light pulses at intensities of 0.7 mW m^{-2} with half-maximal activation already occurring at 0.1 mW m^{-2}.

We next investigated the pathway specificity of UVLamP to verify its use as a $G_{i/o}$ specific optogenetic probe. Three main GPCR pathways are distinguished, that is, $G_{i/o}$, $G_{q11/12/13}$ and G_s.[25] We monitored the $G_{q/11}$ pathway by observing $G_{q/11}$-induced rise in intracellular Ca^{2+} using co-expression of genetically encoded calcium indicators (GECIs) in HEK tsA 201 cells[26] and compared mouse melanopsin with UVLamP (GCamP6m and jRCaMP1b, respectively). We found that blue light stimulation of mouse melanopsin induces a fast rising sustained Ca^{2+} signal, again confirming its capability of modulating the $G_{q/11}$ pathway,[13] whereas UV light stimulation of UVLamP does not lead to a change in intracellular Ca^{2+} (Figure 4A). We also looked at the G_s pathway via G_s-induced rise in intracellular cAMP[27] using co-expression of a red fluorescent protein-based cAMP indicator (Pink Flamindo).[28] We found that UV (or blue) light stimulation of UVLamP did not lead to a rise in intracellular cAMP, whereas direct stimulation of the cAMP producing adenylyl cyclase via Forskolin[29] lead to a fast cAMP increase (Figure 4B), that is blocked by activation of UVLamP following compound washout (Figure S8). These results suggest that UVLamP exclusively modulates the $G_{i/o}$ but not the G_q or G_s pathway.

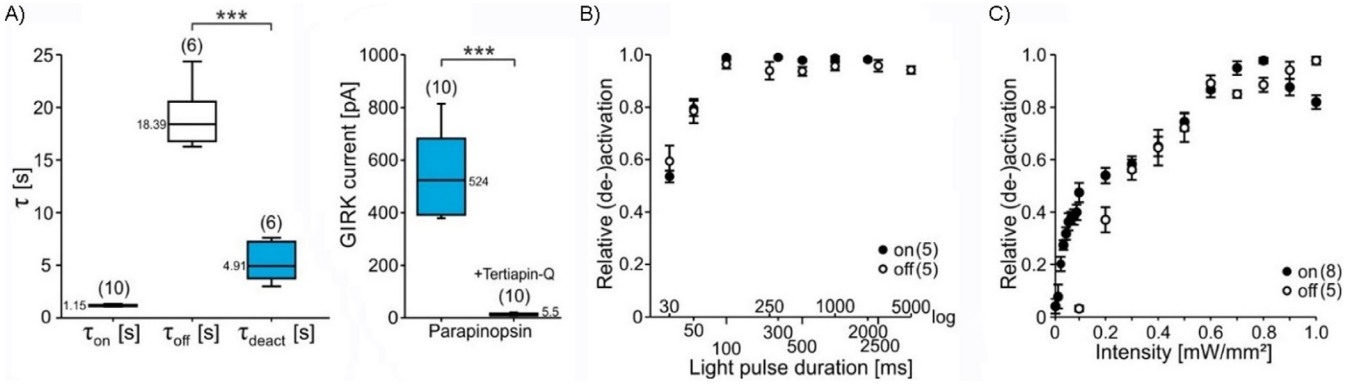

Figure 3. a) Comparison of UV-light-induced activation (τ_{on}), unstimulated dark-adapted inactivation (τ_{off}) and blue-light-induced deactivation (τ_{deact}) time constants for UVLamP (left). Light-induced GIRK currents with and without addition of GIRK channel blocker Tertiapin-Q (right). b) Light pulse duration dependence of UVLamP activation and deactivation. c) Light intensity dependence of UVLamP activation and deactivation.

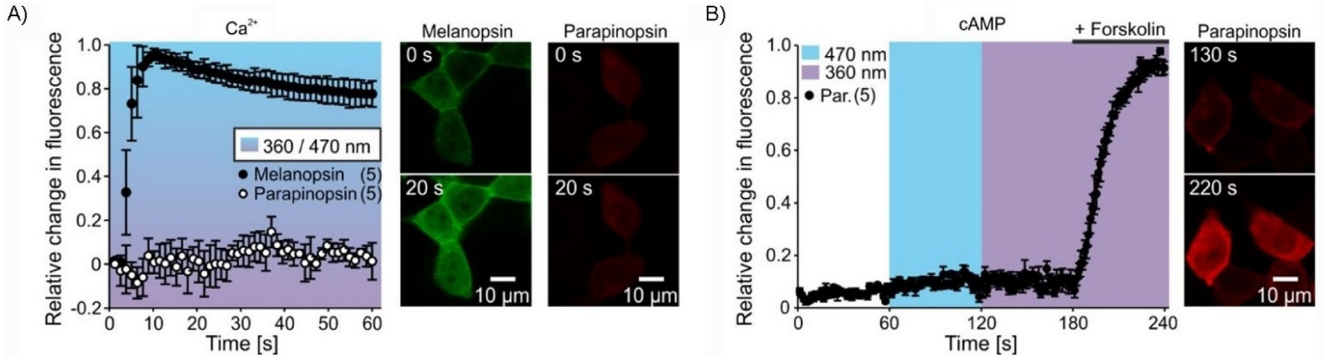

Figure 4. a) Light-induced G_q-mediated Ca^{2+} responses in HEK tsA201 cells for mouse melanopsin (blue light, GCaMP6m, green) and UVLamP (UV light, jRCaMP1b, red). b) Light-induced G_s-mediated intracellular cAMP increase in HEK tsA201 cells for UVLamP (blue and UV light, Pink Flamindo, red). Expressing cells were stimulated with forskolin (activator of adenylyl cyclase) in a final step.

In summary, we present the first experimental prove for the high optogenetic potential of the Japanese lamprey parapinopsin (UVLamP), establishing it as a unique next generation optogenetic tool. We used a hybrid strategy to characterize the biophysical properties of UVLamP and construct its first structural model. Therefore, we combined molecular, cellular, electrophysiological and computational procedures.

In contrast to most other frequently used optogenetic tools, UVLamP enables precise and exclusive control of the $G_{i/o}$ pathway by using millisecond low intensity light pulses for switching this pathway on and most importantly also off. Importantly, UVLamP shows a strongly UV-shifted narrow activation spectrum, enabling combinatory experimental designs with blue-, green-, or red-shifted tools with minimal crosstalk. (Note, red-shifted tools are in principle preferable over blue shifted tools because of the lower energy and deeper tissue penetration of red light.[30]) To our knowledge, UVLamP is the first bistable vertebrate opsin with a positively charged amino acid interacting with the SB in the dark state with this interaction being not relevant for its photoreaction. Additionally, UVLamP allows for long-term activation of the $G_{i/o}$ pathway with millisecond, low intensity light pulses. Due to its bistable nature, UVLamP can also be switched off with a millisecond light pulse in the blue spectrum on demand, leading to highly reduced cellular phototoxicity. UVLamP's unique potential of pathway activation and deactivation by millisecond light pulses is essential for minimizing cellular photodamage due to the high energy UV light.[31] Thus, UVLamP enables new minimally invasive experimental procedures to elucidate GPCR (dis-)function in health and disease.

Because GPCRs coupling to the $G_{i/o}$ pathway are important drug targets for various diseases including anxiety, depression, epilepsy and pain and importantly contribute to synaptic plasticity and neuronal development,[32] our next goals are to engineer UVLamP variants for altered trafficking into disease relevant GPCR domains in the mammalian brain. Because of the unique, blue-shifted, narrow bandwidth features of UVLamP it will now be possible, in combination with other optogenetic tools and genetically encoded sensors, to shed light onto important, unresolved questions in neurobiology, that is, how differently shaped GPCR signals such as fast, transient, long lasting or sustained signals contribute to brain function and change during disease states.[14,33]

Acknowledgements

This work was supported by Deutsche Forschungsgemeinschaft (DFG, German Research Foundation) grants He2471/23-1, He2471/21-1, He2471/19-1, Priority Program (SPP1926) and GE 599/19-1 (to S.H. and K.G.), SFB874 (DFG project no. 122679504) (to S.H.), SFB1280 (DFG project no. 316803389) (to S.H.), Ma5806/2-1 (to M.D.M.), the Individual Research Grant no. 321722360 (GE 599/20-1; to K.G.) and scholarships by Studienstiftung des deutschen Volkes (to D.E.) and Friedrich-Ebert-Stiftung (to R.K.). Further support was provided by the Protein Research Unit Ruhr within Europe (PURE) funded by the Ministry of Innovation, Science and Research (MIWF) of North-Rhine Westphalia, Germany (to K.G.).

Keywords: computational chemistry · electrophysiology · integrative modeling · mutagenesis · optogenetics · structural biology

[1] a) B. V. Zemelman, G. A. Lee, M. Ng, G. Miesenböck, *Neuron* **2002**, *33*, 15; b) X. Li, D. V. Gutierrez, M. G. Hanson, J. Han, M. D. Mark, H. Chiel, P. Hegemann, L. T. Landmesser, S. Herlitze, *Proc. Natl. Acad. Sci. USA* **2005**, *102*, 17816; c) S. Herlitze, L. T. Landmesser, *Curr. Opin. Neurobiol.* **2007**, *17*, 87.
[2] K. Deisseroth, *Nat. Methods* **2011**, *8*, 26.
[3] O. P. Ernst, D. T. Lodowski, M. Elstner, P. Hegemann, L. S. Brown, H. Kandori, *Chem. Rev.* **2014**, *114*, 126.
[4] A. Terakita, *Genome Biol.* **2005**, *6*, 213.
[5] Y. Shichida, T. Matsuyama, *Philos. Trans. R. Soc. London Ser. B* **2009**, *364*, 2881.
[6] M. Murakami, T. Kouyama, *Nature* **2008**, *453*, 363.
[7] E. C. Y. Yan, M. A. Kazmi, Z. Ganim, J.-M. Hou, D. Pan, B. S. W. Chang, T. P. Sakmar, R. A. Mathies, *Proc. Natl. Acad. Sci. USA* **2003**, *100*, 9262.
[8] P. G. de Oliveira, M. L. S. Ramos, A. J. Amaro, R. A. Dias, S. I. Vieira, *Front. Aging Neurosci.* **2019**, *11*, 89.
[9] S. Blackshaw, S. H. Snyder, *J. Neurosci.* **1997**, *17*, 8083.
[10] A. Terakita, M. Koyanagi, H. Tsukamoto, T. Yamashita, T. Miyata, Y. Shichida, *Nat. Struct. Mol. Biol.* **2004**, *11*, 284.
[11] a) E. Kawano-Yamashita, M. Koyanagi, S. Wada, H. Tsukamoto, T. Nagata, A. Terakita, *PLoS One* **2015**, *10*, e0141280; b) S. Wada, B. Shen, E.

Kawano-Yamashita, T. Nagata, M. Hibi, S. Tamotsu, M. Koyanagi, A. Terakita, *Proc. Natl. Acad. Sci. USA* **2018**, *115*, 11310.
[12] M. Koyanagi, E. Kawano, Y. Kinugawa, T. Oishi, Y. Shichida, S. Tamotsu, A. Terakita, *Proc. Natl. Acad. Sci. USA* **2004**, *101*, 6687.
[13] K. Spoida, D. Eickelbeck, R. Karapinar, T. Eckhardt, M. D. Mark, D. Jancke, B. V. Ehinger, P. König, D. Dalkara, S. Herlitze, et al., *Curr. Biol.* **2016**, *26*, 1206.
[14] S. A. Tennigkeit, R. Karapinar, T. Rudack, M.-A. Dreier, P. Althoff, D. Eickelbeck, T. Surdin, M. Grömmke, M. D. Mark, K. Spoida, et al., *ChemBioChem* **2019**, *20*, 1766.
[15] O. A. Masseck, K. Spoida, D. Dalkara, T. Maejima, J. M. Rubelowski, L. Wallhorn, E. S. Deneris, S. Herlitze, *Neuron* **2014**, *81*, 1263.
[16] M. D. Mark, S. Herlitze, *Eur. J. Biochem.* **2000**, *267*, 5830.
[17] B. Hille, *Trends Neurosci.* **1994**, *17*, 531.
[18] a) A. J. Emanuel, M. T. H. Do, *Neuron* **2015**, *85*, 1043; b) V. I. Govardovskii, N. Fyhrquist, T. Reuter, D. G. Kuzmin, K. Donner, *Visual Neurosci.* **2000**, *17*, 509.
[19] T. Okada, M. Sugihara, A.-N. Bondar, M. Elstner, P. Entel, V. Buss, *J. Mol. Biol.* **2004**, *342*, 571.
[20] M. A. Wall, D. E. Coleman, E. Lee, J. A. Iñiguez-Lluhi, B. A. Posner, A. G. Gilman, S. R. Sprang, *Cell* **1995**, *83*, 1047.
[21] D. E. Coleman, S. R. Sprang, *Biochemistry* **1998**, *37*, 14376.
[22] S. Blackshaw, S. H. Snyder, *J. Neurosci.* **1999**, *19*, 3681.
[23] M. Nakagawa, T. Iwasa, S. Kikkawa, M. Tsuda, T. G. Ebrey, *Proc. Natl. Acad. Sci. USA* **1999**, *96*, 6189.
[24] J. Rodgers, S. N. Peirson, S. Hughes, M. W. Hankins, *Cell. Mol. Life Sci.* **2018**, *75*, 3609.
[25] S. Offermanns, *Prog. Biophys. Mol. Biol.* **2003**, *83*, 101.
[26] a) A. H. Partridge, I. E. Smith, R. B. Rumble, *JOP* **2015**, *11*, 42; b) T.-W. Chen, T. J. Wardill, Y. Sun, S. R. Pulver, S. L. Renninger, A. Baohan, E. R. Schreiter, R. A. Kerr, M. B. Orger, V. Jayaraman, et al., *Nature* **2013**, *499*, 295; c) H. Dana, B. Mohar, Y. Sun, S. Narayan, A. Gordus, J. P. Hasseman, G. Tsegaye, G. T. Holt, A. Hu, D. Walpita, et al., *eLife* **2016**, *5*, e12727.
[27] J. Hanoune, N. Defer, *Annu. Rev. Pharmacol. Toxicol.* **2001**, *41*, 145.
[28] K. Harada, M. Ito, X. Wang, M. Tanaka, D. Wongso, A. Konno, H. Hirai, H. Hirase, T. Tsuboi, T. Kitaguchi, *Sci. Rep.* **2017**, *7*, 7351.
[29] R. H. Alasbahi, M. F. Melzig, *Pharmazie* **2012**, *67*, 5.
[30] C. Ash, M. Dubec, K. Donne, T. Bashford, *Lasers Med. Sci.* **2017**, *32*, 1909.
[31] A. Slominski, J. Pawelek, *Clin. Dermatol.* **1998**, *16*, 503.
[32] A. S. Hauser, M. M. Attwood, M. Rask-Andersen, H. B. Schiöth, D. E. Gloriam, *Nat. Rev. Drug Discovery* **2017**, *16*, 829.
[33] a) K. Spoida, O. A. Masseck, E. S. Deneris, S. Herlitze, *Proc. Natl. Acad. Sci. USA* **2014**, *111*, 6479; b) D. Eickelbeck, R. Karapinar, A. Jack, S. T. Suess, R. Barzan, Z. Azimi, T. Surdin, M. Grömmke, M. D. Mark, K. Gerwert, et al., *Commun. Biol.* **2019**, *2*, 60.

Manuscript received: August 5, 2019
Accepted manuscript online: August 29, 2019
Version of record online: October 30, 2019

CHEMBIOCHEM

Supporting Information

Lamprey Parapinopsin ("UVLamP"): a Bistable UV-Sensitive Optogenetic Switch for Ultrafast Control of GPCR Pathways

Dennis Eickelbeck,*[a] Till Rudack,[b, c] Stefan Alexander Tennigkeit,[b, c] Tatjana Surdin,[a] Raziye Karapinar,[a] Jan-Claudius Schwitalla,[a] Brix Mücher,[a] Maiia Shulman,[b, c] Marvin Scherlo,[b, c] Philipp Althoff,[b, c] Melanie D. Mark,[a] Klaus Gerwert,*[b, c] and Stefan Herlitze[a]

cbic_201900485_sm_miscellaneous_information.pdf

Experimental procedure

Generation of plasmid constructs

To construct adeno-associated virus (AAV) expression vectors and allow for the necessary large packaging capacity, the pAAV-CW3SL-EGFP vector (GenBank accession number: KJ411916.2) was used as the backbone plasmid for all opsin constructs [1]. The Japanese lamprey parapinopsin (*Lethenteron camtschaticum*, GenBank accession number: AB116380.1, as submitted to GenBank in 2003 [2]) cDNA was inserted into the vector removing the stop-codon and adding a c-terminal eGFP as a fluorescence marker. This construct will be named parapinopsin or UVLamP in the following. Each element was PCR amplified with 16bp overhangs and inserted into the backbone via AQUA Cloning for expression under the CMV promoter [3]. The mouse melanopsin control plasmid was generated accordingly exchanging the eGFP for an mCherry fluorescence tag, as described in our previous publication [4]. The green and red Ca^{2+} sensors GCaMP6m and jRCaMP1b as well as the red cAMP indicator Pink Flamindo were used unmodified as described in their respective publications [5].

Cell culture and *in vitro* imaging

Human embryonic kidney (HEK) tsA201 cells and HEK GIRK 1/2 cells (HEK293 cells stably expressing GIRK1/2 subunits, kindly provided by Dr. A. Tinker UCL London, GB) were maintained at 37 °C in Dulbecco's modified Eagle's medium (DMEM), 4.5 g l^{-1}D-glucose, supplemented with 10% fetal bovine serum (Gibco) and penicillin/streptomycin in a humidified incubator under 5% CO_2. Growth medium of stable cell lines was supplemented with G418 (5 mg/ml). Cells were cultured on 35 mm glass bottom dishes (for imaging) or plastic bottom dishes (for electrophysiology). Cells were transfected with UVLamP or mouse melanopsin via FuGENE® HD (Promega) according to the manufacturer's protocol and incubated for 18-24 h before recordings. For opsin experiments 9-cis retinal was added to a final medium concentration of 1 µM. To image Ca^{2+} signals in HEK tsA201cells via GCaMP6m or jRCaMP1b, cells were transiently co-transfected with UVLamP + jRCaMP1b or mouse melanopsin + GCaMP6m. Cells were seeded into poly L-lysine coated 35 mm glass bottom dishes, transfected at 70% confluency with equal amounts of plasmid DNA and used the next day. Ca^{2+} and cAMP imaging was performed at an inverted Leica TCS SP5 confocal laser-scanning microscope, (Leica DMI6000 B, Wetzlar, Germany) interfaced to a personal computer, running Leica Application Suite Advanced Fluorescence software (LAS AF 2.6). A 20X/0.7NA objective was used to acquire timelapse images (512 x 512 pixels with 1.2 s interval for live cell imaging). Cells were visualized via mCh or eGFP fluorescence with the 561 nm or 476 nm laser lines. Mouse melanopsin was activated and GCaMP6m was monitored with the 476 and 495 nm argon laser lines, whereas UVLamP was activated/deactivated and jRCaMP1b or Pink Flamindo was monitored with the 405 nm, 476 and 561 nm laser lines. The exact stimulation protocol is shown in the corresponding figure. The adenylyl cyclase activator Forskolin (Tocris, 100 µM) was bath applied at the last step of each stimulation. Fluorescence intensity of the respective sensor signal was measured over time for individual cells, normalized and scaled to the maximal response amplitude. Captured images were transferred into ImageJ software (1.47v; NIH) and analyzed with the time series analyzer V3 plugin.

In vitro electrophysiology

For GIRK channel recordings light sensitive GPCRs were expressed in HEK GIRK 1/2 cells (see above). Cells were cultured on 35 mm dishes and recorded in dark room conditions after transfection. GIRK-mediated K^+-currents were measured and analyzed as described in the following (see also [6]). The external solution was as follows: 20 mM NaCl, 120 mM KCl, 2 mM $CaCl_2$, 1 mM $MgCl_2$, 10 mM HEPES-KOH, pH 7.3 (KOH). Patch pipettes (2–5 MΩ) were filled with internal solution: 100 mM potassium aspartate, 40 mM KCl, 5 mM MgATP, 10 mM HEPES-KOH, 5 mM NaCl, 2 mM EGTA, 2 mM $MgCl_2$, 0.01 mM GTP, pH 7.3 (KOH). Cells were recorded in external solution containing 1µM 9-cis retinal (Sigma). The high affinity GIRK channel blocker Tertiapin-Q (Tocris, 1 µM) was bath applied while recording positive cells in whole-cell patch clamp configuration. Experiments were conducted with an inverted

microscope (Axiovert, ZEISS) and patch pipettes were controlled with a multi-micromanipulator (MPC-325, SUTTER INSTRUMENT). Transfected cells were visualized and UVLamP was manipulated with a monochromator system (Polychrome V, TILL Photonics). The stimulation protocols consisted of 100 ms, 360 nm, 0.7 mW/mm² light pulses for activation and 100 ms, 470 nm, 0.7 mW/mm² light pulses for deactivation if not stated otherwise in the corresponding figures. For the characterization of UVLamP wavelength dependence, light pulse duration dependence and intensity dependence, protocols were pseudorandomized and UVLamP was maximally deactivated between each trial. Whole-cell patch clamp recordings of HEK cells were performed, digitized at 10 kHz and filtered with an EPC10 USB amplifier (HEKA). Series resistances were partially compensated between 70 and 90%. The PatchMaster software (HEKA) was used for monochromator and voltage controls as well as data acquisition, and off-line analysis was made with Igor Pro 6.0 software (Wavemetrics).

Statistics

Statistical significance, test procedure and numbers of cells and/or trials performed (n) are specified in the figure legends. Statistical significance in all experiments was evaluated using SigmaPlot software (Systat Software) or Igor Pro software (WaveMetrics). For all results, the level of significance was set to $p < 0.05$. Statistical significance is indicated with *** $p < 0.001$; ** $p < 0.01$; * $p < 0.05$; n.s. (not significant).

Molecular mechanics simulations

The constructed model was prepared as starting structure for molecular mechanics (MM) simulations in the Moby program suite [7]. Structure preparation included dihedral-, angle-, and bond corrections according to the united atom Amber84 force field [8]. MM simulations were performed according to our previous publications [9,10]. We used the OPLS/AA all atom force field and GROMACS version (2019.3) [11]. All Systems were initially solvated following the Vedani-type [12] and thoroughly solvated in a cubic simulation cell with TIP4P water [13] and 154 mM NaCl. Membrane insertion was performed by using lambada [14] (to calculate a hydrophobic belt) and g_membed [14] (to embed the protein in the membrane).

Model construction software

The VMD [15] plugin QwikMD [16] was used to set up and conduct interactive molecular dynamics (iMD) simulations and molecular dynamics flexible fitting (MDFF) runs employing NAMD [17] with the CHARMM36 force field [18]. We also used Rosetta [19–21] for *ab initio* structure prediction. Modeller [22] was employed for homology modeling. A detailed description of the modeling workflow is given below under Model construction and Model validation.

Model construction strategy

We used our recently developed hybrid modeling workflow [10] to generate a structural model of the Japanese lamprey parapinopsin (GenBank accession number: AB116380.1). The key benefit of this concept is to streamline and facilitate the usage of *ab* inito structure prediction and homology modeling in combination with molecular dynamics simulations. The basis for the model is the bovine rhodopsin crystal structure (PDB-ID 1u19) [23]. The employed sequence alignment for homology modeling in shown in Figure S2. We incorporated additional information about helical regions, which we identified using *ab initio* structure prediction with Rosetta [19–21], structure prediction meta server like constrained consensus topology prediction server (CCTOP) [24] and the Bioinformatics Toolkit [25], as well as homology modeling server like Swiss Model [26] and Lomets [27]. All results are summarized in Figure S3 and the finally used secondary structure is highlighted in green within Figure S2. Conserved functional elements serve as anchor residues considered as residues in the helical region that are identical within a multiple sequence alignment marked with bold stars in Figure S2. For the multiple sequence alignment we used the Glucagon-like peptide1 receptor (PDB-ID 5VAI [28]), the Calcitonin receptor (PDB-ID 5UZ7 [29]), the Beta-2 adrenergic receptor (PDB-ID 3SN6 [30]), the Bos taurus Rhodopsin (PDB-ID 3DQB [31]), and the Squid rhodopsin (PDB-ID 2Z73 [32]).
The X-ray structure of the heterotrimeric G_i protein (PDB-ID 1gp2 [33]) from rat served as basis to construct human GDP bound $G\alpha_o$. As it was shown that the GDP bound state of $G\alpha_i$ has an

Mg^{2+} bound to GDP we added the Mg^{2+} including the three coordinating water molecules and replaced the side chain of Ser47 and the loop from residue number 176 to 183 including the Mg^{2+} coordinating Thr181 using the X-ray structure of the isolated Gα subunit with bound Mg^{2+} (PDB-ID 1bof [34]). Then, the resulting rat G_i protein with bound GDP and Mg^{2+} was used as template to build the homology model of human G_o protein employing SCWRL 4.0 [35]. The sequence alignments of all three G protein subunits are shown in Figures S4-6.
The complex with the G protein was constructed based on the β2AR crystal structure (PDB-ID 3SN6 [30]). The parapinopsin model was aligned with β2AR and our G protein model with the one of the X-ray structure. As helix 5 and 6 from parapinopsin clash with the Gα subunit we used QwikMD [16] to run an interactive molecular dynamics simulation using NAMD [17] through VMD [15] to move these two helices outwards. We assume that the overall shape between the β2AR and the G_s protein is highly similar to the shape of the parapinopsin G protein complex. Therefore, we refined the parapinopsin G protein complex to the shape of β2AR using molecular dynamics flexible fitting (MDFF) simulations [36]. The X-ray structure of β2AR (PDB-ID 3SN6 [30]) was converted into a volumetric density using volutiles of VMD [15]. QwikMD [16] was used to set up and conduct MDFF runs employing NAMD [17] with the CHARMM36 force field [18]. We constructed the melanopsin G_o protein complex following the same strategy as described for parapinopsin. We used the uncomplexed melanopsin model from Tennigkeit et al. [10] and the same GDP bound G protein as used for parapinopsin.
Within the iterative process that involves Monte Carlo based (Rosetta) [19–21] and MD based structure optimization (Moby-program package (H. Höweler, MAXIMOBY, CHEOPS, Altenberge, Germany, 2007)) the final model of parapinopsin in complex with human G_o is solvated, placed into the membrane and optimized regarding, side chain orientation, and hydrogen bond network. Then, the model is equilibrated by MM simulations (Gromacs 2019.3 [11]) to adapt to its physiological environment.

Model validation
Table S1 reflects a high sequence similarity of 70 % (identity 42 %) for the helical area of parapinopsin compared to bovine rhodopsin. A correct alignment is further ensured by the above described anchor residues. In addition, the key functional region, the retinal binding pocket, contains highly conserved functionally relevant amino acids. Based on these values we expect a highly accurate homology model of parapinopsin. The rat G_i and human G_o protein have an almost identical sequence (Figures S4-6), therefore, we also expect a highly reliable G protein model. Figure S7 shows the convergency to a stable plateau of the RMSD within our 475 ns MD simulations of the parapinopsin G_o protein complex and the melanopsin G_i protein complex. This convergency reflects that both simulation systems have reached a stable conformation.

Supplementary Table and Figures

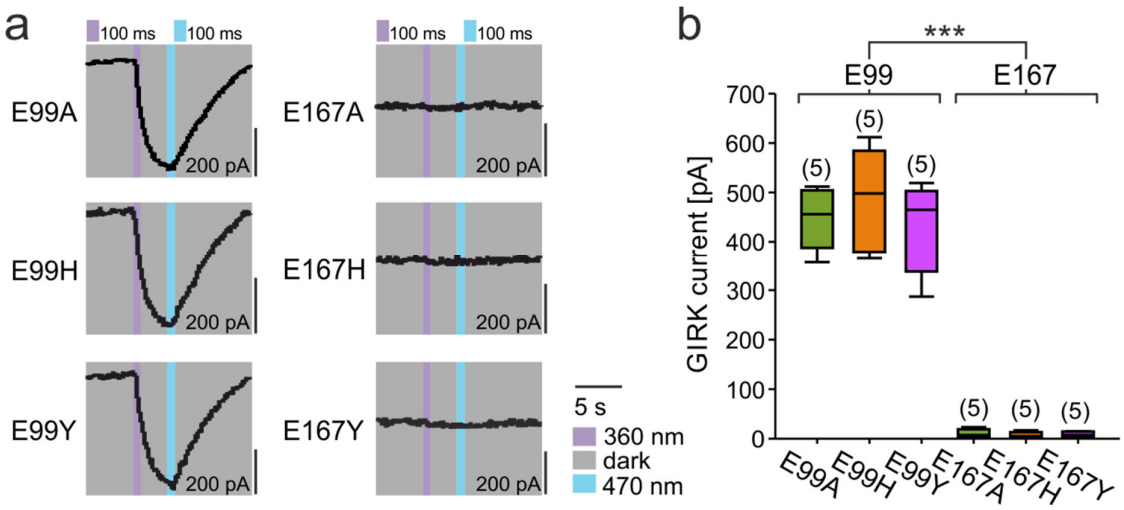

Figure S1. *In vitro* characterization of japanese lamprey parapinopsin ("UVLamP") counterion point mutations via whole-cell patch clamp recordings of GIRK currents in HEK GIRK 1/2 cells. a) Example traces of light induced induced GIRK currents for UVLamP E99A/H/Y and E167A/H/Y point mutants. b) Light induced GIRK currents for UVLamP E99A/H/Y and E167A/H/Y point mutants.

Table S1. Sequence identity and similarity of parapinopsin and bovine rhodopsin. Data are given in %.

%	All	No Ter	H1-8	H1	H2	H3	H4	H5	H6	H7	H8
Identity	39	41	42	23	43	46	33	35	56	60	55
Similarity	66	67	70	58	60	71	71	62	81	90	73

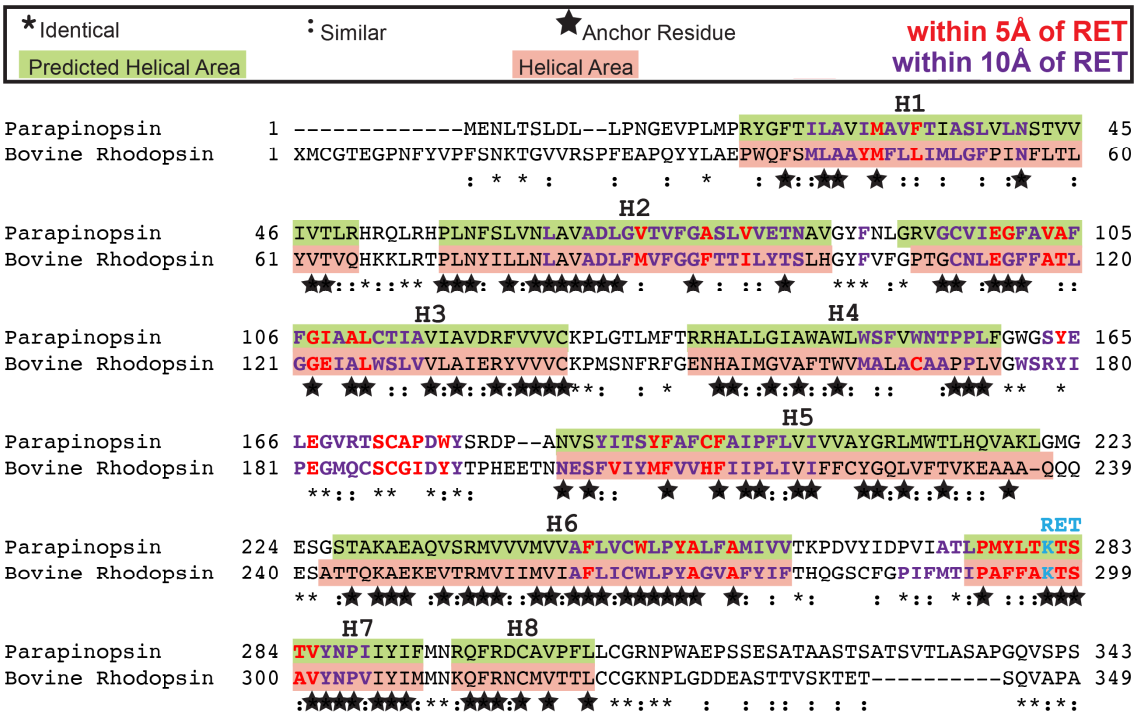

Figure S2. Parapinopsin model construction. Sequence alignment of parapinopsin with bovine rhodopsin [23]. The residues within 5 Å distance around the retinal are marked red and between 5 to 10 Å are purple. The predicted helices are highlighted in green and the helical residues of the X-ray structures in light red.

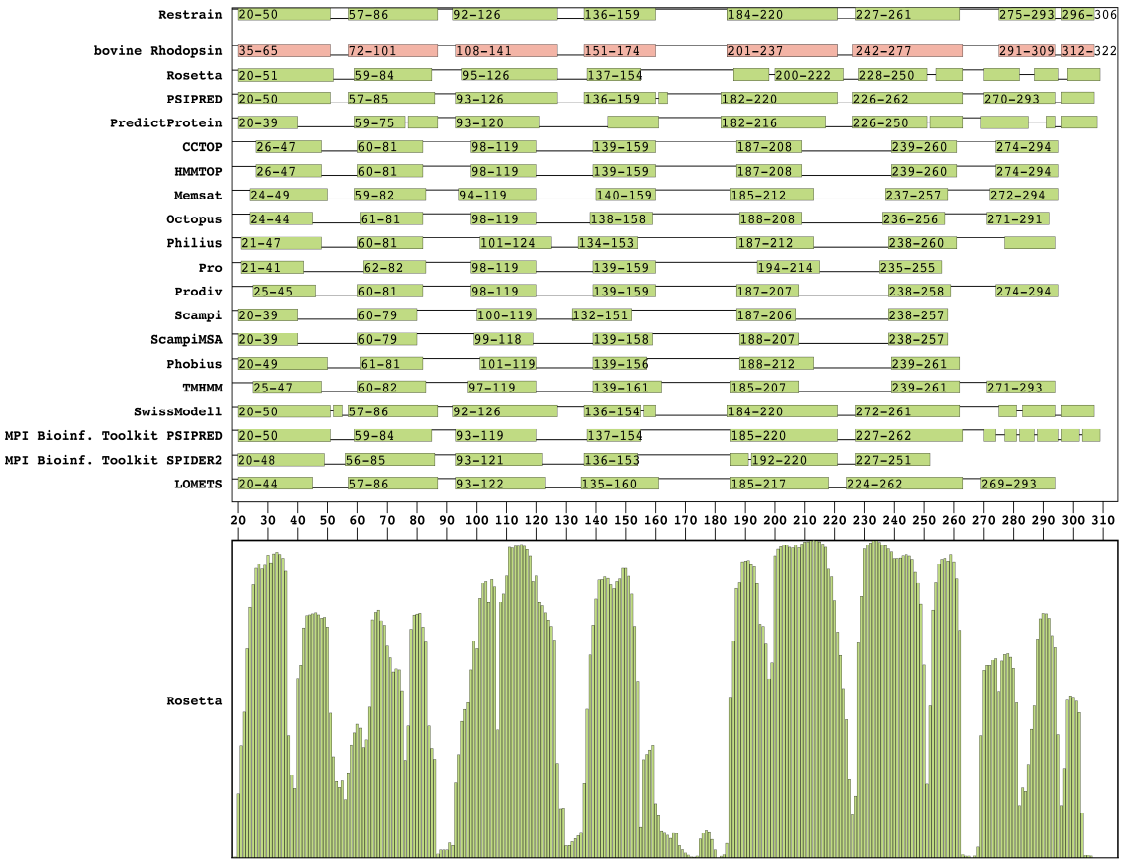

Figure S3. Secondary structure prediction of parapinopsin. The top illustrates the secondary structure prediction results for parapinopsin and the bottom represents the results of the rosetta secondary structure prediction for the same template. All results were merged and included as restrains in the calculation of the homology model. The helical area of the bovine rhodopsin crystal structure (PDB-ID 1u19 [23]) is colored in light red.

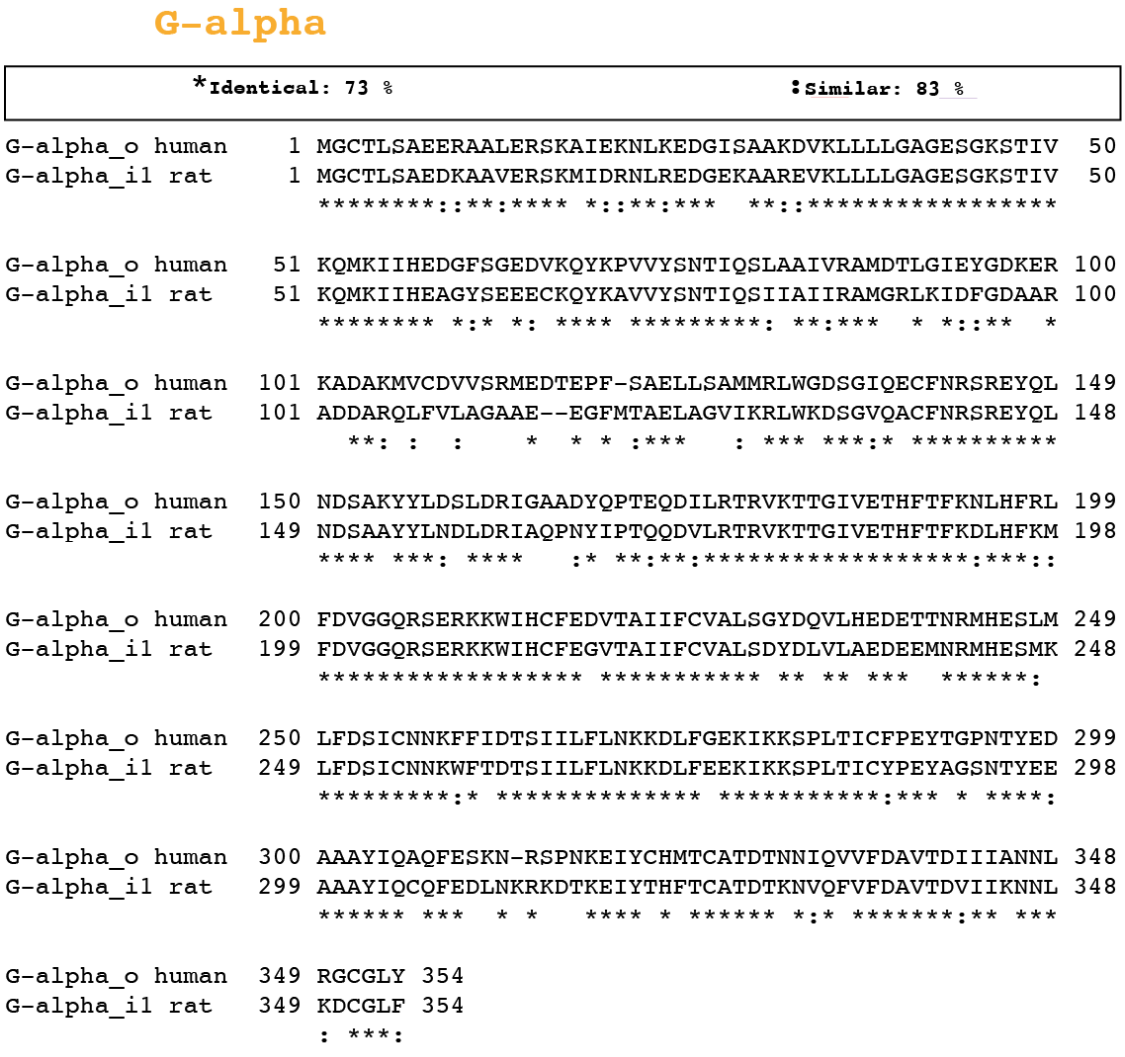

Figure S4. Sequence alignment of $G\alpha_{i/o}$. Shown is the sequence alignment between $G\alpha_i$ rat (PDB-ID: 1GP2 [33])and $G\alpha_o$ human (UNIPROT-ID: P09471).

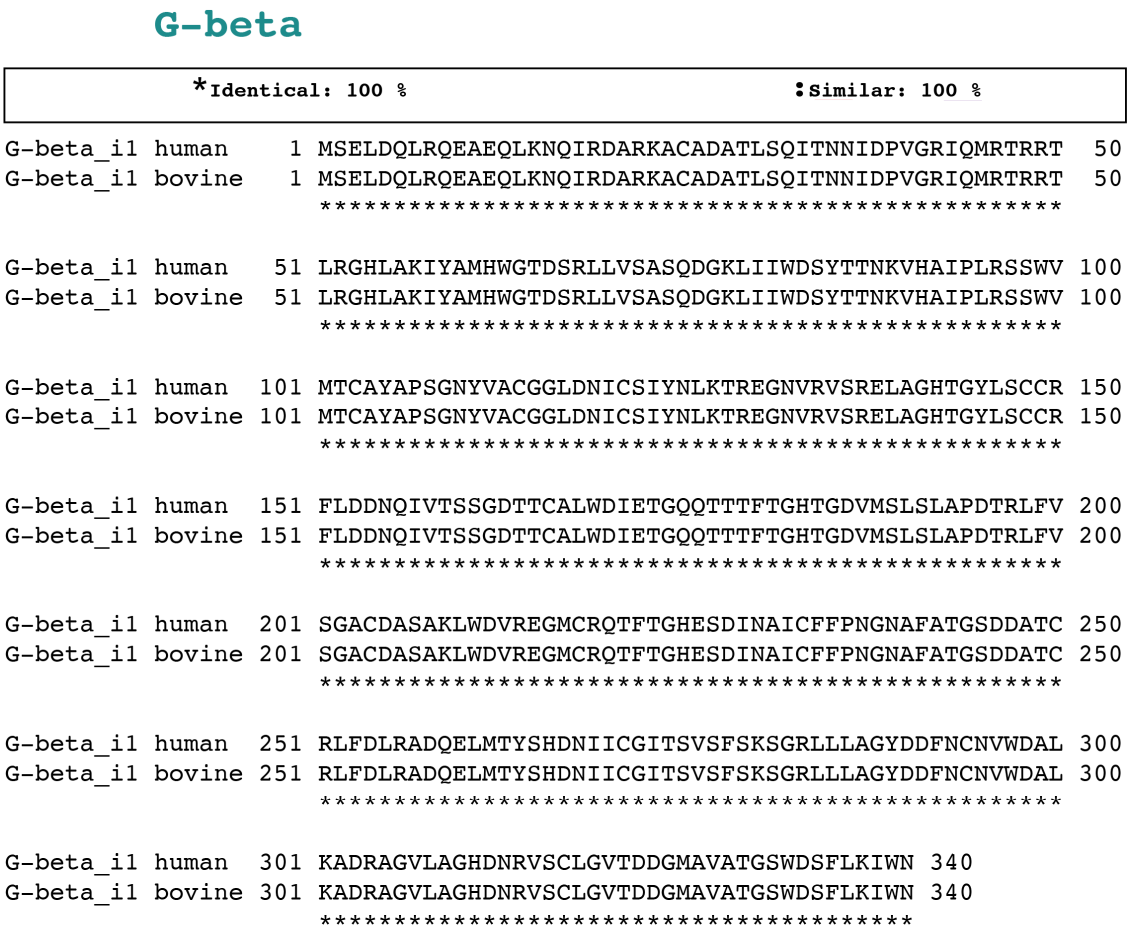

Figure S5. Sequence alignment of Gβ. Shown is the sequence alignment between Gβ1 bovine (PDB-ID 1GP2 [33]) and Gβ1 human (UNIPROT-ID: P62873).

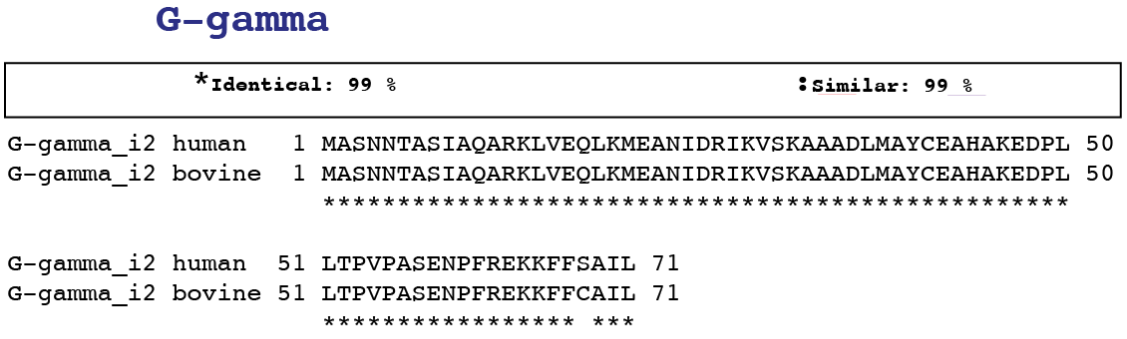

Figure S6. Sequence alignment of Gγ. The sequence alignment between Gγ2 bovine (PDB-ID 1GP2 [33]) and Gγ2 human (UNIPROT-ID: P59768) is represented.

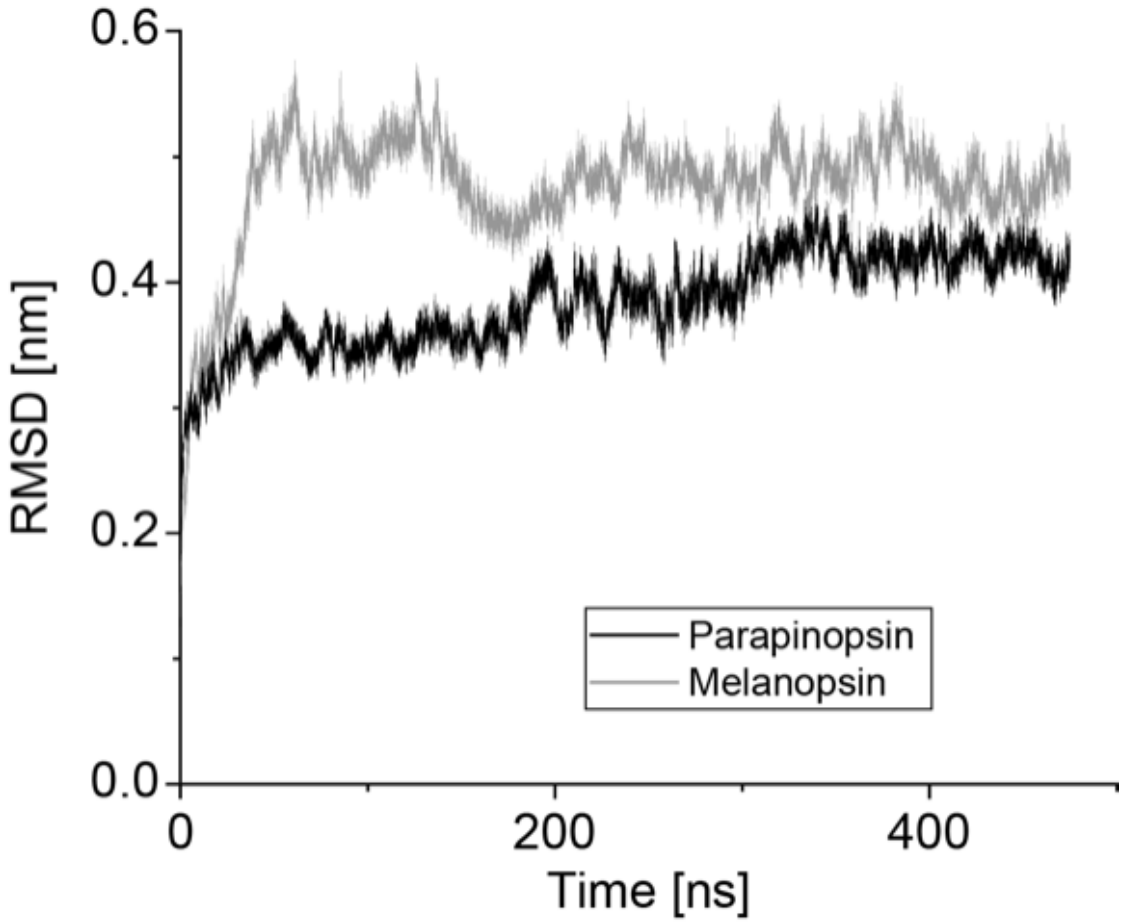

Figure S7. RMSD of the MM simulations based on our constructed models. Shown is the RMSD of the Cα-atoms of the equilibration MM simulations for parapinopsin (black) and melanopsin (light gray). All illustrated RMSDs are stable.

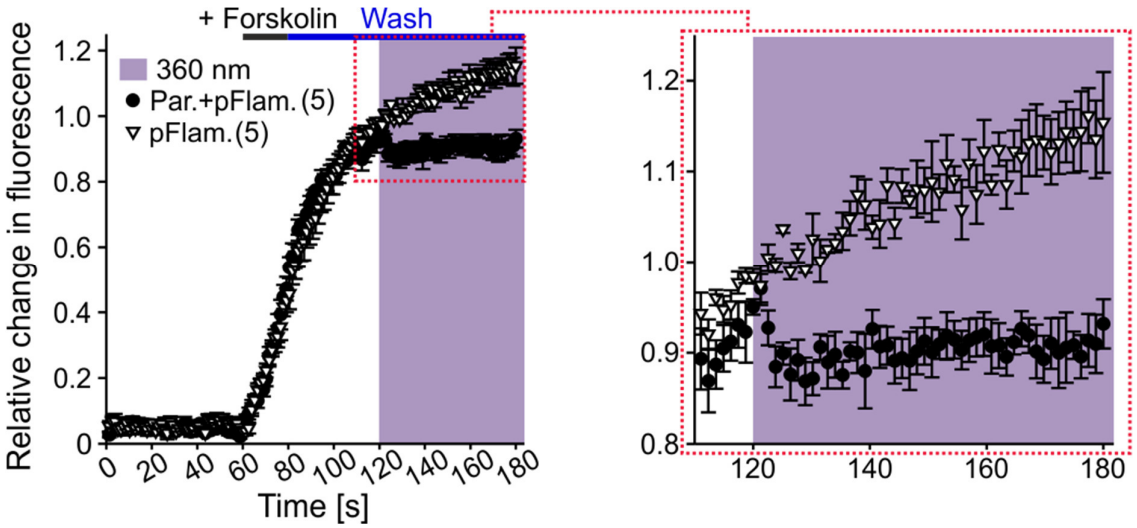

Figure S8. Light induced blockage of Gs mediated intracellular cAMP increase in HEK tsA201 cells for UVLamP (UVLaMP + Pink Flamindo) vs. Control (Pink Flamindo). Cells were stimulated with Forskolin/UV light and compound was washed out as indicated.

References

[1] J.-H. Choi, N.-K. Yu, G.-C. Baek, J. Bakes, D. Seo, H. J. Nam, S. H. Baek, C.-S. Lim, Y.-S. Lee, B.-K. Kaang, *Mol. Brain* **2014**, *7*, 17.

[2] a) A. Terakita, M. Koyanagi, H. Tsukamoto, T. Yamashita, T. Miyata, Y. Shichida, *Nat. Struct. Mol. Biol.* **2004**, *11*, 284; b) M. Koyanagi, E. Kawano, Y. Kinugawa, T. Oishi, Y. Shichida, S. Tamotsu, A. Terakita, *PNAS* **2004**, *101*, 6687.

[3] H. M. Beyer, P. Gonschorek, S. L. Samodelov, M. Meier, W. Weber, M. D. Zurbriggen, *PLoS One* **2015**, *10*, e0137652.

[4] K. Spoida, D. Eickelbeck, R. Karapinar, T. Eckhardt, M. D. Mark, D. Jancke, B. V. Ehinger, P. König, D. Dalkara, S. Herlitze et al., *Curr. Biol.* **2016**, *26*, 1206.

[5] a) T.-W. Chen, T. J. Wardill, Y. Sun, S. R. Pulver, S. L. Renninger, A. Baohan, E. R. Schreiter, R. A. Kerr, M. B. Orger, V. Jayaraman et al., *Nature* **2013**, *499*, 295; b) H. Dana, B. Mohar, Y. Sun, S. Narayan, A. Gordus, J. P. Hasseman, G. Tsegaye, G. T. Holt, A. Hu, D. Walpita et al., *eLife* **2016**, *5*; c) K. Harada, M. Ito, X. Wang, M. Tanaka, D. Wongso, A. Konno, H. Hirai, H. Hirase, T. Tsuboi, T. Kitaguchi, *Sci. Rep.* **2017**, *7*, 7351.

[6] X. Li, D. V. Gutierrez, M. G. Hanson, J. Han, M. D. Mark, H. Chiel, P. Hegemann, L. T. Landmesser, S. Herlitze, *PNAS* **2005**, *102*, 17816.

[7] U. Höweler, *MAXIMOBY, CHEOPS, Altenberge, Germany*, **2007**.

[8] L. Yang, Å. A. Skjevik, W.-G. Han Du, L. Noodleman, R. C. Walker, A. W. Götz, *Data Brief* **2016**, *8*, 1209.

[9] a) K. Eisenhauer, J. Kuhne, E. Ritter, A. Berndt, S. Wolf, E. Freier, F. Bartl, P. Hegemann, K. Gerwert, *J. Biol. Chem.* **2012**, *287*, 6904; b) J. Kuhne, K. Eisenhauer, E. Ritter, P. Hegemann, K. Gerwert, F. Bartl, *Angew. Chem., Int. Ed. Engl.* **2015**, *54*, 4953; c) J. Kuhne, J. Vierock, S. A. Tennigkeit, M.-A. Dreier, J. Wietek, D. Petersen, K. Gavriljuk, S. F. El-Mashtoly, P. Hegemann, K. Gerwert, *PNAS* **2019**, *116*, 9380.

[10] S. A. Tennigkeit, R. Karapinar, T. Rudack, M.-A. Dreier, P. Althoff, D. Eickelbeck, T. Surdin, M. Grömmke, M. D. Mark, K. Spoida et al., *ChemBioChem* **2019**, *20*, 1766.

[11] M. J. Abraham, T. Murtola, R. Schulz, S. Páll, J. C. Smith, B. Hess, E. Lindahl, *SoftwareX* **2015**, *1-2*, 19.

[12] A. Vedani, D. W. Huhta, *J. Am. Chem. Soc.* **1991**, *113*, 5860.

[13] a) W. L. Jorgensen, J. Chandrasekhar, J. D. Madura, R. W. Impey, M. L. Klein, *J. Chem. Phys.* **1983**, *79*, 926; b) H. W. Horn, W. C. Swope, J. W. Pitera, J. D. Madura, T. J. Dick, G. L. Hura, T. Head-Gordon, *J. Chem. Phys.* **2004**, *120*, 9665.

[14] T. H. Schmidt, C. Kandt, *J. Chem. Inf. Model.* **2012**, *52*, 2657.

[15] W. Humphrey, A. Dalke, K. Schulten, *J. Mol. Graphics* **1996**, *14*, 33.

[16] J. V. Ribeiro, R. C. Bernardi, T. Rudack, J. E. Stone, J. C. Phillips, P. L. Freddolino, K. Schulten, *Sci. Rep.* **2016**, *6*, 26536.

[17] J. C. Phillips, R. Braun, W. Wang, J. Gumbart, E. Tajkhorshid, E. Villa, C. Chipot, R. D. Skeel, L. Kalé, K. Schulten, *J. Comput. Chem.* **2005**, *26*, 1781.

[18] J. Huang, A. D. MacKerell, *J. Comput. Chem.* **2013**, *34*, 2135.

[19] A. Leaver-Fay, M. Tyka, S. M. Lewis, O. F. Lange, J. Thompson, R. Jacak, K. Kaufman, P. D. Renfrew, C. A. Smith, W. Sheffler et al., *Methods Enzymol.* **2011**, *487*, 545.

[20] K. W. Kaufmann, G. H. Lemmon, S. L. Deluca, J. H. Sheehan, J. Meiler, *Biochemistry* **2010**, *49*, 2987.

[21] S. Lindert, J. A. McCammon, *J. Chem. Theory Comput.* **2015**, *11*, 1337.

[22] A. Sali, T. L. Blundell, *J. Mol. Biol.* **1993**, *234*, 779.

[23] T. Okada, M. Sugihara, A.-N. Bondar, M. Elstner, P. Entel, V. Buss, *J. Mol. Biol.* **2004**, *342*, 571.

[24] M. Stemmer, T. Thumberger, M. Del Sol Keyer, J. Wittbrodt, J. L. Mateo, *PLoS One* **2015**, *10*, e0124633.

[25] L. Zimmermann, A. Stephens, S.-Z. Nam, D. Rau, J. Kübler, M. Lozajic, F. Gabler, J. Söding, A. N. Lupas, V. Alva, *J. Mol. Biol.* **2018**, *430*, 2237.

[26] T. Schwede, J. Kopp, N. Guex, M. C. Peitsch, *Nucleic Acids Res.* **2003**, *31*, 3381.

[27] S. Wu, Y. Zhang, *Nucleic Acids Res.* **2007**, *35*, 3375.

[28] Y. Zhang, B. Sun, D. Feng, H. Hu, M. Chu, Q. Qu, J. T. Tarrasch, S. Li, T. Sun Kobilka, B. K. Kobilka et al., *Nature* **2017**, *546*, 248.
[29] Y.-L. Liang, M. Khoshouei, M. Radjainia, Y. Zhang, A. Glukhova, J. Tarrasch, D. M. Thal, S. G. B. Furness, G. Christopoulos, T. Coudrat et al., *Nature* **2017**, *546*, 118.
[30] S. G. F. Rasmussen, B. T. DeVree, Y. Zou, A. C. Kruse, K. Y. Chung, T. S. Kobilka, F. S. Thian, P. S. Chae, E. Pardon, D. Calinski et al., *Nature* **2011**, *477*, 549.
[31] P. Scheerer, J. H. Park, P. W. Hildebrand, Y. J. Kim, N. Krauss, H.-W. Choe, K. P. Hofmann, O. P. Ernst, *Nature* **2008**, *455*, 497.
[32] M. Murakami, T. Kouyama, *Nature* **2008**, *453*, 363.
[33] M. A. Wall, D. E. Coleman, E. Lee, J. A. Iñiguez-Lluhi, B. A. Posner, A. G. Gilman, S. R. Sprang, *Cell* **1995**, *83*, 1047.
[34] D. E. Coleman, S. R. Sprang, *Biochemistry* **1998**, *37*, 14376.
[35] G. G. Krivov, M. V. Shapovalov, R. L. Dunbrack, *Proteins* **2009**, *77*, 778.
[36] L. G. Trabuco, E. Villa, K. Mitra, J. Frank, K. Schulten, *Structure* **2008**, *16*, 673.

Author contributions

D.E., R.K., S.A.T., T.R. and S.H. conceived and analyzed experiments. T.S. and R.K. generated plasmid constructs. D.E., R.K., J.S. and B.M. performed cell culture assays. D.E. conducted cell culture electrophysiology experiments. S.A.T. and T.R., together with M.Sh., M.Sc. and P.A., performed biophysical modelling experiments and created the modelling figures. D.E. designed the figures and wrote the manuscript with input and detailed descriptions from all authors for their specific contributions.